Low-Strength Type I Interferon Signaling Promotes CAR T-Cell Treatment Efficacy

Erting Tang[1,#], Yifei Hu[1,2,#], Guoshuai Cao[1], Nicholas W. Asby[1], Duy-Thuc Nguyen[1], Nada S. Aboelella[5], Hanna Ruiz[1], Yu Zhao[1], Lishi Xie[3], Xiufen Chen[3], Michael R. Bishop[5,6], Peter A. Riedell[5,6], James L. LaBelle[5], Justin P. Kline[3,4,5,6], Jun Huang[1,3,4,*]

[1]Pritzker School of Molecular Engineering, University of Chicago, Chicago, IL 60637, USA

[2]Pritzker School of Medicine, University of Chicago, Chicago, IL 60637, USA

[3]Committee on Immunology, University of Chicago, Chicago, IL 60637, USA

[4]Committee on Cancer Biology, University of Chicago, Chicago, IL 60637, USA

[5]Section on Hematology/Oncology, Department of Medicine, University of Chicago, Chicago, IL 60637, USA

[6]The David and Etta Jonas Center for Cellular Therapy, University of Chicago, Chicago, IL 60637, USA

[#]These authors contributed equally.

*Correspondence to: huangjun@uchicago.edu

ABSTRACT

CD19-directed chimeric antigen receptor (CAR) T-cell therapy has significantly advanced the treatment landscape for relapsed/refractory diffuse large B-cell lymphoma (r/r DLBCL). However, up to 60% of patients do not achieve a complete response. To uncover determinants of therapeutic efficacy, we analyzed the infusion products of eight r/r DLBCL patients with distinct clinical responses to axicabtagene ciloleucel using single-cell transcriptomics. Compared to patients who exhibited progressive disease, infusion products of complete responders demonstrated enriched signatures of type I interferon (IFN-I) signaling. Based on these findings, we developed a novel strategy to improve CD19-directed CAR T-cell treatment efficacy by incorporating IFN-I as an enhancer during the ex vivo manufacturing process. For both CD28- and 4-1BB-costimulated second-generation CARs, we found that low-strength IFN-I signaling enhanced CAR T-cell cytotoxicity and in vivo efficacy. On the other hand, high-strength IFN-I signaling compromised cell viability and in vivo efficacy. Our low-strength IFN-I signaling approach leverages an existing FDA-approved pharmacologic agent and is compatible with current CAR constructs and manufacturing workflows. Together, our results establish IFN-I as a potent and costimulation-independent enhancer of CAR T-cell efficacy and provide a translationally feasible approach to enhance CAR T-cell therapies for r/r DLBCL.

Key Words: chimeric antigen receptor (CAR), type I interferon (IFN-I), axicabtagene ciloleucel (axi-cel), lisocabtagene maraleucel (liso-cel), diffuse large B-cell lymphoma (DLBCL)

INTRODUCTION

Chimeric antigen receptor (CAR) T-cell therapy has advanced the standard-of-care for hematologic malignancies, achieving complete response rates ranging 39-71% across relapsed/refractory diffuse large B-cell lymphoma (r/r DLBCL)[1], acute lymphoblastic leukemia[2], and multiple myeloma[3,4]. However, the therapy's effectiveness is constrained by significant rates of treatment failure. In r/r DLBCL, only ~40% of patients exhibit a complete response, whereas the remaining ~60% of patients exhibit a partial response, stable disease, or progressive disease, as defined by the International Working Group response criteria.[1] Patients who cannot clear their lymphoma burden have limited therapeutic options and often succumb to their disease.

Existing studies have correlated treatment failure with diminished CAR T-cell polyfunctionality[5], increased T-cell exhaustion signatures within CAR T-cell products[6–8], inhibition by CAR Tregs[9], as well as failure of CAR T cells to persist and expand in vivo[1,10], among others[11]. Given the importance of CAR T-cell-intrinsic factors in determining treatment outcomes, we investigated the infusion products (IP) of CAR T-cell therapy patients with r/r DLBCL using single-cell transcriptomics. We observed that, compared to patients with progressive disease, the IPs of complete responders demonstrated enriched signatures of type I interferon (IFN-I) signaling. This observation was also validated using an independent, published dataset from Maus et al.[12]

As potent immunomodulators, IFN-I cytokines have long been of interest for their potential to modulate immunotherapy response rates.[13,14] Upon binding to type I interferon receptors (IFNAR), IFN-I cytokines trigger a phosphorylation cascade that activates transcription factors such as signal transducer and activator of transcription 1 (STAT1), STAT2, and interferon regulatory factor 9 (IRF9).[13] These transcription factors coordinate transcription of interferon-stimulated genes, such as *IRF7*, *MX1*, *ISG15*, *ISG20*, *IFITM1/2/3* which mediate antiviral immunity and effector functions.[13,15] In $CD8^+$ T cells, IFN-I signaling enhances cytotoxicity[16] and induces central memory differentiation[17], while also controlling T-cell exhaustion[18], inhibitory

65 receptor expression[19], and apoptosis[20,21]. Due to their immunomodulatory effects, clinical
66 formulations of IFN-I cytokines (e.g., Avonex, Intron A, Alferon N) have been approved by the
67 FDA for the treatment of malignancies (e.g., hairy cell leukemia, follicular lymphoma)[22],
68 autoimmune diseases (e.g., multiple sclerosis)[23], and viral infections (e.g., hepatitis B and C)[24].
69 Despite being an attractive FDA-approved cytokine for regulating immune functions in cancer,
70 autoimmunity, and infection, IFN-I has not been utilized to modulate CAR T-cell therapy responses.
71 Given our bioinformatic discoveries and the literature-established roles of T-cell-intrinsic
72 IFN-I signaling in modulating T-cell differentiation and functionality[13], we hypothesize that IFN-I
73 signaling enhances CAR T-cell efficacy during the ex vivo manufacturing process. In this study,
74 we detail our discovery and development of IFN-I cytokines as an enhancer to partially address
75 CAR T-cell therapy failure rates. Through in vitro functional assays and in vivo lymphoma
76 xenograft mouse models, we demonstrate proof-of-principle for a novel ex vivo manufacturing
77 method that leverages low-strength, FDA-approved IFN-I cytokines to improve the in vivo
78 treatment efficacy of CAR T-cell therapy.

RESULTS

Enrichment of IFN-I signaling in infusion products of complete responders.

To uncover determinants of therapeutic efficacy, infusion products from 8 r/r DLBCL patients treated with CD28-costimulated CD19-directed CAR T cell therapy (axicabtagene ciloleucel, "axi-cel") at the University of Chicago Medicine were profiled using single-cell sequencing. The cohort included 5 patients who achieved a complete response (CR) at one month post-infusion and another 3 patients who exhibited progressive disease (N-CR) (**Figure 1a**). After removing low-quality cells, we obtained 27,879 cells distributed among 7 T-cell clusters (**Figure 1b**) based on gene expression (**Figure 1c**, figure S1a). No cluster was patient specific (**Figure 1d**, figure S1b). The two CD8$^+$ clusters were annotated as central memory (CM, *SELL*$^+$*IL7R*$^+$*TBX21*$^-$*KLRG1*$^-$) or effector memory (EM, *SELL*$^-$*IL7R*$^+$*TBX21*$^+$*KLRG1*$^+$) T cells. The two CD4$^+$ clusters were annotated as memory (Mem, *FOXP3*^{lo}*IL7R*$^+$*CTLA4*^{lo}) or regulatory (Treg, *FOXP3*^{hi}*IL7R*$^-$*CTLA4*^{hi}) T cells. The remaining three clusters consisted of naïve-activated (*SELL*$^+$*IL7R*$^+$*TCF7*$^+$*CD38*$^+$), unconventional (*TRDC*$^+$*NCAM1*$^+$) as a mixture of γδ and natural killer phenotypes, and proliferating (*MKI67*$^+$*TOP2A*$^+$) T cells. No discernable composition differences were found between CR and N-CR patients (**Figure 1b**, **d**, figure S1c).

Gene set enrichment analysis revealed distinct differences between CR and N-CR T cells. CR T cells were enriched for signatures of type I interferon signaling ("IFNα response"), cytolysis, and leukocyte degranulation, whereas N-CR T cells were enriched for signatures of cell growth, hypoxia, and glycolysis (**Figure 1e**). Notably, the CR-specific IFNα response signature was enriched in CR T cells across T-cell clusters (**Figure 1f**) and individual patients (**Figure 1g**).

To validate our discovery of CR-specific IFN-I signaling signatures, we tested our findings using an independent and published single-cell transcriptomic dataset from Maus et al. (*n* = 15 patients with lymphoma who received axi-cel, **Figure 1a**).[12] This cohort included 10 patients who

104 achieved a complete response (CR) and 5 who did not (N-CR), as assessed one-month post-
105 infusion. After filtering out low-quality cells, performing dimensionality reduction, and clustering,
106 we uncovered the same 7 T-cell clusters identified in our own dataset (**Figure 1h**) based on gene
107 expression (**Figure 1i**, figure S2a). No cluster was patient specific (**Figure 1j**). Notably, expression
108 of ISGs (including *ISG20*, *IFITM1/3*) was upregulated in IP of CR (figure S2b). Most importantly,
109 IFNα response signatures was enriched in IPs of CR. The CR-specific IFNα response signature
110 was consistently observed across all T-cell clusters except Tregs (**Figure 1k**, figure S2c) and
111 individual patients (**Figure 1l**).
112 Taken together, findings from the discovery and validation datasets strongly support an
113 association between IFN-I signaling and improved CAR T-cell clinical efficacy.
114
115 *IFN-I signaling increases CAR T-cell cytotoxicity.*
116 Previous studies have demonstrated the immunomodulatory role of T cell-intrinsic IFN-I
117 signaling.[13] For instance, IFN-I signaling promotes cytotoxicity[16], T_h1 polarization[25–27], and central
118 memory phenotype differentiation[17], all of which may be desired CAR T-cell characteristics and
119 potentially explain the differential clinical responses observed in the two patient cohorts. Based
120 on these findings and our bioinformatics analyses, we hypothesized that IFN-I signaling can
121 enhance CAR T-cell efficacy. To test this hypothesis, we generated both CD28- and 4-1BB-
122 costimulated CD19-directed CAR T cells from primary human T cells. Our CD28-costimulated
123 CAR is based on axicabtagene ciloleucel (axi-cel, **Figure 2b**), whereas our 4-1BB-costimulated
124 is based on lisocabtagene maraleucel (liso-cel, **Figure 2c**). To induce IFN-I signaling, we treated
125 CAR T cells with exogenous IFN-α2, a highly potent, FDA-approved, and clinically compatible
126 IFN-I subtype, for culturing CAR T cells (**Figure 2a**). Prior to addition of IFN-α2, we confirmed that
127 CAR T cells globally expressed the type I interferon receptor in a transduction-independent and
128 costimulation-independent manner (Figure S3a, c).

129 Since each downstream target of IFN-I signaling exhibits varying sensitivity to IFN-I
130 concentrations[28], we hypothesized that the IFN-I culturing concentration may affect CAR T-cell
131 functions. To determine the IFN-I concentrations for our study, we initially titrated IFN-α2 on both
132 CD28- and 4-1BB-costimulated CAR T cells and measured intracellular interferon regulatory
133 factor 7 (IRF7), a key ISG[29] (figure S3b, d). IFN-I signaling reached saturation at concentrations
134 above 3000 IU/mL of IFN-α2, consistent with previous studies.[16,27] We also observed half-maximal
135 IRF7 upregulation at approximately 100-300 IU/mL of IFN-α2. Consequently, we established
136 three culturing conditions: IFN-α2 at saturating concentration ("IFNα-hi", 3000 IU/mL), IFN-α2
137 near half-maximal effective concentration ("IFNα-lo", 300 IU/mL), and no IFN-α2 ("IFNα-neg", 0
138 IU/mL). We confirmed that these conditions resulted in concentration-dependent upregulation of
139 ISGs, including *MX1*, *IRF7*, and *ISG15* (figure S4).
140 CAR T cells were treated based on the three culturing conditions for downstream
141 experimentation (**Figure 2a**). Since IFN-I signaling can inhibit viral transduction[30], we chose to
142 add IFN-α2 after CAR transduction, which enabled us to achieve consistent transduction
143 efficiency and expression of both CD28-costimulated (**Figure 2d**, **f**) and 4-1BB-costimulated
144 CARs (**Figure 2e**, **h**) across the three culturing conditions. Between culturing conditions, IFN-I
145 signaling did not affect CD4/CD8 ratios (**Figure 2g**, **i**), memory phenotypes (figure S5a-d), or IFN-
146 I receptor expression (figure S5e-h). To test cytotoxicity, CAR T cells were co-cultured with OCI-
147 Ly8 target cells, a $CD19^+$ human DLBCL cell line. In both CD28- and 4-1BB-costimulated CAR T
148 cells, we observed IFN-I signaling significantly increased CAR T-cell cytotoxicity (**Figure 2j**, **l**),
149 expression of cytolytic molecules (granzyme B, perforin, **Figure 2k**, **m**), and secretion of cytokines
150 (IL-2, TNF, IFNγ, **Figure 2n-o**), in a concentration-dependent manner. These findings suggest
151 that IFN-I signaling increases CAR T-cell cytotoxicity.
152

153 *High-strength IFN-I signaling increases apoptosis, whereas low-strength IFN-I signaling does not.*
154 After the manufacturing process, both CD28- and 4-1BB-costimulated CAR T cells cultured under
155 the IFNα-hi condition, but not the IFNα-lo condition, consistently yielded fewer viable cells
156 compared to the IFNα-negative condition (**Figure 3a, c**). Given previous reports that IFN-I
157 signaling can inhibit cell proliferation[31], we evaluated whether CAR T-cell proliferation was
158 affected by IFN-I signaling through assessing the proliferation marker, Ki-67. No significant
159 differences in Ki-67 expression were observed across the three culturing conditions, indicating
160 that IFN-I signaling does not impair CAR T-cell proliferation during ex vivo expansion (**Figure 3b,**
161 **d,** figure S6). Since IFN-I signaling also reportedly promotes T-cell apoptosis[20,21], we next
162 quantified CAR T-cell apoptosis via Annexin V staining. Flow phenotyping revealed that CAR T
163 cells in the IFNα-hi condition trended towards increased apoptosis, whereas those in the IFNα-lo
164 condition did not (**Figure 3e-f**).
165 To further investigate the cellularity and apoptosis of CAR T cells from the three culturing
166 conditions following antigen-specific stimulation, we subsequently quantified cellularity and
167 apoptosis of CAR T cells after stimulation with OCI-Ly8 target cells. Following stimulation, CAR
168 T-cell cellularity in the IFNα-lo and IFNα-neg conditions was statistically indistinguishable (**Figure**
169 **3g-h**). On the other hand, CAR T-cell cellularity in the IFNα-hi condition was significantly depleted
170 compared to the other two conditions. At the timepoint when CAR T-cell cellularity in the IFNα-hi
171 condition significantly diverged (day 6 post-stimulation in the representative data), we observed
172 a corresponding enrichment in apoptosis (**Figure 3i-j**).
173 Taken together, these findings suggest that high-strength, but not low-strength IFN-I
174 signaling increases CAR T-cell apoptosis, thereby negatively affecting persistence during both ex
175 vivo expansion and antigen-specific activation.
176

177 *Low-strength IFN-I signaling promotes CAR T-cell treatment efficacy in vivo.*

178 Given that the IFNα-lo condition uniquely increases CAR T-cell functionality (**Figure 2**) without
179 compromising cell viability (**Figure 3**) in both CD28- and 4-1BB-costimulated CAR T cells, our
180 data demonstrate that low-strength IFN-I signaling promotes CAR T-cell efficacy in vitro by
181 balancing function with persistence. Based on these in vitro conclusions, we hypothesized that
182 the IFNα-lo condition uniquely optimizes CAR T-cell treatment efficacy in vivo.

183 To test our hypothesis, we analyzed the efficacy of CAR T cells prepared from the three
184 culturing conditions in a xenograft mouse model based on the OCI-Ly8 cell line (**Figure 4a**). To
185 control for donor-donor heterogeneity, CAR T cells were derived from multiple independent
186 donors (three for CD28-costimulated CAR T cells and two for 4-1BB-costimulated CAR T cells).
187 Across donors, CAR T-cell injection prolonged survival relative to the PBS-only control. For CD28-
188 costimulated CAR T cells with donors 1 and 2, CAR T cells from the IFNα-lo condition significantly
189 prolonged survival and slowed down tumor progression relative to CAR T cells from the IFNα-neg
190 and IFNα-hi conditions (**Figure 4b**, figure S7a). For donor 3, although the differences between
191 CAR T cells from IFNα-lo and IFNα-hi conditions were relatively modest compared to other
192 donors, one mouse treated with CAR-T cells from the IFNα-lo condition showed a significantly
193 better and sustained response (Figure S7b-c). For 4-1BB-costimulated CAR T cells with donors
194 4 and 5, CAR T cells from the IFNα-lo condition consistently yielded superior outcomes compared
195 to CAR T cells from the IFNα-neg and IFNα-hi conditions, leading to improved survival and tumor
196 control (**Figure 4c**, figure S7d). Taken together, our findings support our hypothesis and indicate
197 that CAR T cells generated from the IFNα-lo condition, regardless of costimulatory domain, exhibit
198 enhanced in vivo efficacy compared to those from IFNα-neg or IFNα-hi conditions across multiple
199 donors.

200 In conclusion, our in vitro and in vivo studies support a model in which low-strength IFN-I
201 signaling selectively promotes CAR T-cell treatment efficacy (**Figure 4d**). IFN-I signaling

202 promotes CAR T-cell functionality in a concentration-dependent manner, leading to more effective
203 cytotoxicity, cytokine release, and tumor control. However, at a high enough concentration, IFN-I
204 signaling also increases T-cell apoptosis, leading to reduced yield, poorer persistence, and
205 ineffective tumor control. Although the optimal level of IFN-I signaling may be subject to donor-
206 donor heterogeneity, CAR T cells treated with low-strength IFN-I signaling, regardless of
207 costimulatory domain, consistently exhibit enhanced effector functions without significantly
208 increased apoptosis.

209 **DISCUSSION**

210

211 In this study, we leveraged single-cell transcriptomic analyses of patient IPs from two independent
212 datasets, in vitro functional and phenotypic analyses, and in vivo xenograft mouse studies, to
213 establish that low-strength IFN-I signaling during the ex vivo CAR T-cell manufacturing process
214 selectively promotes CAR T-cell treatment efficacy in vivo in a costimulation-independent manner.
215 Our strategy of harnessing IFN-I signaling to enhance CAR T-cell efficacy is grounded in clinical
216 data and existing literature, while also highlighting IFN-I as an enhancer with significant
217 translational potential for use during the CAR T-cell manufacturing process.

218 There are major attractive qualities that make IFN-I a uniquely promising and translatable
219 enhancer for both CAR T-cell therapy and other emerging cellular therapy modalities. Unlike all
220 other natural and engineered cytokines being developed as CAR T-cell enhancers (including IL-
221 7, IL-10, IL-15, IL-21, Fc-IL-4)[32–36], IFN-Is are uniquely biocompatible drugs with an existing and
222 extensive clinical track record for the treatment of malignancies[22], autoimmune diseases[23], and
223 viral infections[24]. First discovered in the 1950s for their antiviral activities, IFN-I is one of only two
224 cytokines ever approved by the FDA for cancer treatment (the other being IL-2).[37] Biologically,
225 IFN-I elicit a known signaling pathway through the type I interferon receptor to induce antiviral
226 interferon stimulated genes.[13,15] Their pharmacodynamics and pharmacokinetics have been
227 thoroughly explored in pre-clinical and clinical studies.[38] By uniquely employing a biologically,
228 pharmacologically, and clinically characterized pharmacophore, our low-strength IFN-I
229 manufacturing method is straightforward and less likely to introduce uncharacterized toxicities.
230 We also point out that our method was mechanistically inspired by bioinformatics findings from
231 clinical biospecimens, thereby recapitulating a physiological and clinically relevant phenotype.

232 In terms of basic biology, we found that IFN-I signaling enhances CAR T-cell cytotoxicity
233 in a dose-dependent manner; however, excessively strong IFN-I signaling also increases
234 apoptosis, thereby reducing persistence. Our findings are compatible with existing literature on T-

235 cell-intrinsic effects of IFN-I signaling. Enhancement of cytotoxicity and type I cytokine secretion
236 among $CD8^+$ and $CD4^+$ T cells after culturing with exogenous IFN-I is well-established.[16,39]
237 Moreover, the field's current understanding is that T-cell-intrinsic IFN-I signaling leads to different
238 consequences, depending on whether TCR stimulation temporally precedes ("in-sequence") or
239 follows ("out-of-sequence") IFN-I signaling.[13,40] In-sequence signaling generally enhances T-cell
240 functions, while out-of-sequence signaling generally does the opposite.[13] In our studies, since T-
241 cell activation (via CD3/CD28 Dynabeads) preceded IFN-I treatment, our CAR T cells were
242 subject to in-sequence signaling under the current paradigm. Moreover, our findings mirror the
243 expected consequences of in-sequence IFN-I signaling. Lastly, the concentration-dependent
244 nature of our model is compatible with other studies demonstrating that different cellular functions
245 exhibit varying sensitivities to IFN-I signaling.[28]

246 Our findings may also reconcile the currently obscure relationship between IFN-I signaling
247 and CAR T-cell function. On one hand, Jung et al. and Evgin et al. reported that IFN-I signaling
248 hinders CAR T-cell efficacy.[21,41] Both groups subjected their CAR T cells to IFN-β, which has up
249 to 30-fold higher affinity for the type I interferon receptor compared to IFN-α2.[42] Taking into
250 account their high-affinity IFN-I subtype and culturing concentrations, their conditions are similar
251 to our IFNα-hi condition, which accounts for their negative findings. On the other hand, Zhao et
252 al. reported that IFN-I signaling enhances CAR T-cell efficacy.[43] We reason their positive findings
253 are due to their CAR T cells receiving a weak IFN-I stimulus, since they did not add exogenous
254 IFN-I in their in vitro system. In conclusion, our model demonstrates a non-linear relationship
255 between IFN-I signaling and CAR T-cell efficacy, thereby potentially reconciling these intriguing
256 prior studies.

257 Our study advances the understanding of IFN-I signaling in T cells and lays the foundation
258 for translational applications in CAR-T cell therapies, though several avenues remain for
259 exploration. While our experiments generated CAR-T cells from healthy donors for mechanistic
260 studies, future research should focus on using T cells from cancer patients. Since cancers often

261 suppress IFN-I signaling to evade immune detection and weaken IFN-I-driven immune
262 responses[44–46], modulating IFN-I signaling in cancer patient-derived CAR-T cells may yield
263 significantly improved therapeutic effects. Furthermore, we tested only two IFN-I concentrations,
264 emphasizing the need for more rigorous dosing studies to determine the optimal therapeutic
265 window. Finally, although our study focused on IFN-α2 due to its clinical relevance, it underscores
266 the broader potential of the IFN-I family, with many subtypes still underexplored and potentially
267 capable of further enhancing CAR-T cell functionality through cytokine modulation.

268 **METHODS**

269

270 *Collection of patient biospecimens*

271 Deidentified patient biospecimens were gathered in accordance with ethical guidelines under the
272 institutional review board at the University of Chicago Medicine. Residual infusion product cells
273 were collected from the patient's infusion product bag and stored in CELLBANKER 1 (Amsbio,
274 11888). Cells were cryopreserved in liquid-phase nitrogen.

275

276 *Single-cell RNA-seq data generation.*

277 Cryopreserved biospecimens were thawed and washed with cold FACS buffer (PBS, 2% BSA,
278 0.05% sodium azide). Antibody-stained cells were conjugated with LIVE/DEAD Fixable Near-IR
279 viability dye (Invitrogen, L34975) at 1:1000 dilution in PBS for 5 minutes at room temperature.
280 Finally, cells were washed 3x in cold cell media (RPMI, 10% FBS) before sorting (BD Biosciences,
281 FACSAria Fusion) for live cells. Sorted cells were partitioned into droplets for single-cell RNA-seq
282 via Chromium Next GEM Single-Cell 5'Kit v2 (10x Genomics, 1000263). RNA-seq libraries were
283 prepared according to manufacturer protocols. Libraries were quantified via the Qubit dsDNA HS
284 Assay Kit (Invitrogen, Q32851), quality-checked for fragment sizes via high-sensitivity D5000
285 screentapes (Agilent, 5067-5592), pooled, and sequenced (Illumina, Novaseq-6000 and Nextseq-
286 550).

287

288 *Single-cell RNA-seq data analysis.*

289 Alignment, filtering, counting, and demultiplexing of RNA-seq reads were performed using the
290 Cell Ranger *count* (10x Genomics, version 7.1.0). For alignment, the GRCh38 reference genome
291 was appended with the CAR transgene sequence of axicabtagene ciloleucel.

292 Downstream analysis was performed using Seurat[47] (version 4.3.0). After converting count
293 matrices and merging all Seurat objects, we filtered cells with >15% mitochondrial reads and
294 40,000 UMIs to remove debris, doublets, and dead cells. The matrix was normalized using
295 *NormalizeData* with default options. The top 5,000 variable genes found by *FindVariableFeatures*
296 with the default "vst" method were taken as variable genes. Data were centered and scaled using
297 *ScaleData*, with additional regression against (1) the percent of mitochondrial RNA content and
298 (2) difference in cell cycle S-phase and G2M-phase scores. Scaled data were then used for
299 principal component analysis (PCA) using *RunPCA*. Data harmonization to remove patient-
300 specific effects was performed on the principal components using Harmony[48] (version 0.1.1)
301 through *RunHarmony*. Top 50 harmony components were used for Uniform Manifold and
302 Projection (UMAP) dimensionality reduction via *RunUMAP*. The same harmony components were
303 used to construct the shared nearest neighbor (SNN) graph using *FindNeighbors*, which was then
304 partitioned to identify clusters using *FindClusters* with the "original Louvain" algorithm.
305 Differentially expressed genes were determined using *FindMarkers* in Seurat package
306 with default parameters. Gene set enrichment analysis and pathway enrichment analysis were
307 carried out using clusterProfiler[49] (version 4.6.2) based on pathways from the msigdbr database's
308 built-in msigdbr[50] package (version 7.5.1). Gene module scores were calculated for each cell
309 using *AddModuleScore* in Seurat for msigdbr or customized gene sets.
310
311 *Lentiviral production and transduction.*
312 CD28- or 4-1BB-costimulated anti-CD19 human CARs were designed based on the sequences
313 of axi-cel or liso-cel. The axi-cel sequence was obtained from a previously published sequencing
314 study,[51] while the liso-cel sequence was retrieved from the Global Substance Registration System
315 database (UNII: 7K2YOJ14X0). A GFP-tagged, CD28-costimulated or 4-1BB-costimulated, anti-
316 CD19 human CAR was cloned onto the pHR vector backbone to constitute the transfer plasmid.
317 Plasmids were transfected into the Lenti-X 293T packaging cell line (Takara, 632180) for lentiviral

318 production. In brief, Lenti-X 293T cells were seeded and grown overnight to ~90% confluence.
319 Subsequently, transfer, packaging (psPAX2), and envelope (pMD2.G) plasmids were co-
320 transfected into Lenti-X 293T cells via Lipofectamine 3000 (Invitrogen, L3000001). After 72 hours,
321 the viral supernatant was collected and stored at -80°C until transduction. During transduction,
322 lentiviruses were added to human primary T cells along with protamine sulfate (Millipore Sigma,
323 P3369-10G) to a final concentration of 10 µg/mL. Cells were spinoculated at 800 x *g* for 60
324 minutes at room temperature.
325
326 *CAR T-cell production and culturing.*
327 PBMC samples were collected from healthy donors under an Institutional Review Board approved
328 protocol. Cryopreserved human PBMCs were thawed in warm T-cell media (RPMI supplemented
329 with 10% FBS, 1% penicillin/streptomycin, 2 mM L-glutamine, and 50 µM 2-mercaptoethanol).
330 Subsequently, PBMCs were cultured for 3 hours in complete T-cell media (T-cell media
331 supplemented with 50 units/mL of IL-2) in order to allow monocytes to adhere to the culture flask.
332 The non-adhered cells were transferred to a new culture flask. Cells were counted via the LUNA-
333 FL cell counter. T-cell percentage (% $CD3^+$) was calculated by flow cytometry.
334 T cells were seeded in complete T-cell media at 0.75 x 10^6/mL. CD3/CD28 Dynabeads
335 (Gibco, 11161D) were washed and added at 1:1 ratio. After overnight activation, T cells were
336 transduced with CAR lentiviruses (MOI of 5). The media was refreshed after 24 hours with
337 complete T-cell media dosed with recombinant human IFN-α2 (BioLegend, 592702). T cells were
338 subsequently expanded, and media was refreshed every 2 days.
339
340 *Quantitative reverse transcription PCR.*
341 CAR T cells were treated under IFN-I culturing conditions for 24 hours. Then, cells were collected,
342 and stained for viability (Invitrogen, L34975). Live CAR T cells were sorted (BD Biosciences,
343 FACSAria Fusion). Total RNA was extracted using the Monarch Total RNA Miniprep Kit (NEB,

344 T2010S), according to manufacturer protocols. RNA was quantified via the Qubit RNA HS Assay
345 Kit (Invitrogen, Q32852). cDNA was synthesized using the GoScript Reverse Transcription
346 System (Promega, A5000).

347 Quantitative PCR was performed using Taqman Gene Expression Assay (ThermoFisher
348 Scientifc, 4331182) and Applied Biosystems TaqMan Universal PCR Master Mix (ThermoFisher
349 Scientifc, 4304437), on LightCycler® 96 Instrument (Roche). The cycling conditions were as
350 follows: UNG incubation at 50°C for 2 minutes, initial denaturation at 95°C for 10 minutes, followed
351 by 40 cycles of denaturation at 95°C for 15 seconds and annealing/extension at 60°C for 60
352 seconds. Each sample was run in triplicate.

353 The specific Taqman Gene Expression Assay used were as follows: *ACTB*
354 (Hs01060665_g1), *IRF7* (Hs01014809_g1), *MX1* (Hs00895608_m1), and *ISG15*
355 (Hs01921425_s1). Relative gene expression levels were calculated using the 2^-ΔΔCt method,
356 with *ACTB* serving as the internal control. Statistical analysis was performed using one-way
357 ANOVA followed by a Tukey's post hoc test for significance.

358

359 *In vitro co-culture immunoassays.*

360 For all co-culture immunoassays, CAR T cells (E) and luciferized OCI-Ly8 cells (T) were seeded
361 under a fixed E/T ratio. To measure in vitro cytotoxicity, co-cultures were established with E/T
362 ratio of 1:1. After 6 hours, One-Glo Luciferase substrate (Promega, E6110) was added to each
363 well. Residual tumor cells were quantified via luciferase activity. As a positive control, target cells
364 were directly lysed with 1% NP-40 (Abcam, ab142227). To measure cytotoxic molecule
365 expression, co-cultures were established with E/T ratio of 1:1 with 1x brefeldin A (BioLegend,
366 420601). After 4 hours, cells were collected for intracellular staining and flow cytometry. To
367 measure cytokine secretion, co-cultures were established with E/T ratio of 1:1. After 24 hours, the
368 culture supernatant was collected and stored. Secreted cytokines were quantified using
369 LEGENDplex immunoassays per manufacturer's protocol (BioLegend). To measure in vitro

370 persistence, co-cultures were established with E/T ratio of 1:5. Every three days, cells were
371 counted using Precision Count Beads (BioLegend, 424902) and measured for apoptosis on flow
372 cytometry. Cell media was then refreshed.
373
374 *Flow cytometry.*
375 Cells were washed with cold FACS buffer (PBS, 2% BSA, 0.05% sodium azide). Fc receptors
376 were blocked by incubation with Human TruStain FcX (BioLegend, 422301) at 1:50 dilution for 5
377 minutes at 4°C. Then, cells were incubated for 30 minutes at 4°C in the dark with an antibody
378 staining solution for surface antigen staining . Antibodies were used according to manufacturer
379 recommendations. After staining, cells were incubated briefly either with live/dead staining
380 solution or apoptosis staining solution for 10 minutes at room temperature. Then, cells were either
381 washed and resuspended in FACS buffer or resuspended in Annexin V Binding Buffer (BioLegend,
382 422201). Cells were ready for analysis by flow cytometry or intracellular staining.
383 For intracellular staining, cells stained for surface antigens were subject to the BD
384 Fixation/Permeabilization Kit (BD Biosciences, 554714) for cytotoxic molecule staining or True-
385 Nuclear™ Transcription Factor Buffer Set (BioLegend, 424401) for IRF7 staining, following
386 manufacturer recommendations. In brief, Cells were fixed in fixation buffer, washed 3x in
387 permeabilization buffer, and incubated for 60 minutes at 4°C in the dark with a staining solution
388 containing antibodies and permeabilization buffer. After staining, cells were washed 2x in
389 permeabilization buffer, 1x in FACS buffer, and resuspended in FACS buffer for analysis by flow
390 cytometry.
391 For Ki-67 staining, cells stained for surface antigens were washed 2x in PBS, fixed in
392 prechilled 70% ethanol overnight, washed 2x in FACS buffer, and incubated for 30 minutes at 4°C
393 in the dark with Ki-67 antibody staining solution. After staining, cells were washed 2x in FACS
394 buffer, and resuspended in FACS buffer for analysis by flow cytometry.

395 Flow cytometry was performed on LSRFortessa (BD Biosciences) or Aurora (Cytek
396 Biosciences). Data were analyzed using FlowJo software (version 10.10.0).
397
398 *Antibody panels.*
399 All antibodies were used according to manufacturer recommendations. APC-anti-IFNAR2 (10359-
400 MM07T-A) was from Sino Biological. All other antibodies originate from BioLegend. For surface
401 staining, AF647-anti-CD3 (clone: UCHT1, 300416), BV421-anti-CD3 (clone: UCHT1, 300434),
402 BV510-anti-CD4 (clone SK3, 344633), PerCP/Cy5.5-anti-CD8α (clone SK1, 344709), PE-anti-
403 CD45RA (clone HI100, 304107), BV421-anti-CD45RO (clone UCHL1, 304223), and AF647-anti-
404 CCR7 (clone G043H7, 353217) were used. For intracellular staining, PE/Cy7-anti-granzyme B
405 (clone QA16A02, 372213), PE-anti-perforin (clone B-D48, 353303), and PE-anti-IRF7 (clone
406 12G9A36, 656003) were used. For live/dead staining, Zombie NIR Fixable Viability Kit (423106)
407 was used in PBS. For apoptosis staining, BV421-Annexin V (640923) or PE/Cy7-Annexin V
408 (640950) was diluted in Annexin V Binding Buffer (422201). For Ki-67 staining, PE-anti-Ki-67
409 (clone Ki-67, 350503) was used.
410
411 *Lymphoma xenograft mouse model.*
412 Immunocompromised NOD *scid* IL2Rgamma^{null} (NSG, Strain #005557) mice were purchased
413 from JAX and maintained at the animal resource center (ARC) of the University of Chicago in
414 accordance with institutional guidelines. Mice were monitored daily. Care and experimental
415 procedures were carried out in line with the Institutional Animal Care and Use Committee (IACUC)
416 approved protocols of the Animal Care Center at the University of Chicago.
417 5×10^6 OCI-Ly8-Chili-luc cells in 100 μL PBS were intravenously injected into 8-12-week-
418 old NSG mice to build a xenograft lymphoma model. 5×10^5 or 1×10^6 CAR T cells were
419 intravenously injected 1 week later. Lymphoma progression was monitored using either IVIS
420 Spectrum (PerkinElmer) or Lago X (Spectral Instruments Imaging) following the Intraperitoneal

injection of D-luciferin potassium (PerkinElmer, 122799). Animals were anesthetized at 2% isoflurane throughout acquisition. Bioluminescence was quantified with Aura software (Spectral Instruments Imaging). Mice were euthanized upon manifestation of paralysis, impaired mobility, or poor body condition (BCS<2).

Statistical analysis.

Statistical tests were performed on R (version 4.2.1) or GraphPad Prism 10 (version 10.1.1). Comparisons between two groups were performed using Wilcoxon Rank-Sum test. Comparisons between more than two groups were performed by either one-way or two-way ANOVA followed by Tukey correction for multiple comparisons. Survival data were analyzed using the Log-Rank (Mantel-Cox) test. To assess correlation, Spearman's rank correlation coefficient was calculated, as indicated.

Data availability.

All data are available from the authors upon reasonable request.

Code availability.

Codes supporting the analyses performed in this study are available at https://github.com/ertingtang/IFN-I-CART.

440 **ACKNOWLEDGEMENTS**

441

442 We thank the NIH New Innovator award (1DP2AI144245) and NIH R21AI169159 for financial
443 support (to J.H.). Y.H. was supported by the University of Chicago MSTP Training Grant
444 (T32GM007281). N.W.A. was supported by the University of Chicago MTCR training grant
445 (T32CA009594). Flow cytometry was performed at the Cytometry and Antibody Technology
446 Facility at University of Chicago, which receives financial support from the Cancer Center Support
447 Grant (P30CA014599). Live bioluminescence imaging was performed at the University of Chicago
448 Integrated Small Animal Imaging Research Resource. We thank the UChicago Blood Donation
449 Center for healthy donor PBMCs. We thank Aniruddhsingh Solanki at the animal resource center
450 at University of Chicago for excellent technical assistance.

AUTHOR CONTRIBUTIONS

Y.H. and E.T. designed the study, designed experiments, analyzed and interpreted data and wrote the manuscript. J.H. supervised the project and edited the manuscript. E.T., G.C., Y.Z. performed single-cell analyses. Y.H., generated single-cell patient data. Y.H., E.T., and N.W.A. performed in vitro experimentation. E.T., D.N., N.S.A, and Y.H. performed in vivo studies. P.A.R. coordinated patient biospecimens for these studies. All authors contributed intellectually or assisted with experiments in this manuscript.

459 **DECLARATIONS OF INTERESTS**

460

461 J.H., Y.H., and E.T. are listed as inventors on a patent related to interferon-enhanced CAR-T cells
462 (US provisional patent application 63/789,043). J.L.L. reports other grants from AbbVie and the
463 American Cancer Society outside the submitted work. No disclosures were reported by the other
464 authors. P.A.R. reports Research Support/Funding: BMS, Kite Pharma, Inc./Gilead, MorphoSys,
465 Calibr, Tessa Therapeutics, Fate Therapeutics, Xencor, and Novartis Pharmaceuticals
466 Corporation. Speaker's Bureau: Kite Pharma, Inc./Gilead; Consultancy on advisory boards:
467 AbbVie, Novartis Pharmaceuticals Corporation, BMS, Janssen, BeiGene, Karyopharm
468 Therapeutics Inc., Takeda Pharmaceutical Company, Kite Pharma, Inc./Gilead, Sana
469 Biotechnology, Nektar Therapeutics, Nurix Therapeutics, Intellia Therapeutics, and Bayer.
470 Honoraria: Novartis Pharmaceuticals Corporation. M.R.B. reports Membership on an Advisory
471 Board or Consultancy for Kite/Gilead, Novartis, CRISPR Therapeutics, Autolus Therapeutics,
472 BMS, Incyte, Sana Biotechnology, Iovance Biotherapeutics. He has served on a Speakers Bureau
473 for BMS, Kite/Gilead, Agios, and Incyte. J.P.K. receives research support from Merck, Verastem,
474 and iTeos; has served on a speaker's bureau for Kite/Gilead; and has served on advisory boards
475 for Verastem, Seattle Genetics, MorphoSys, and Karyopharm.

476 **REFERENCES**

477

478 1. Neelapu, S. S. *et al.* Axicabtagene Ciloleucel CAR T-Cell Therapy in Refractory Large B-
479 Cell Lymphoma. *N. Engl. J. Med.* **377**, 2531–2544 (2017).
480 2. Maude, S. L. *et al.* Tisagenlecleucel in Children and Young Adults with B-Cell
481 Lymphoblastic Leukemia. *N. Engl. J. Med.* **378**, 439–448 (2018).
482 3. Rodriguez-Otero, P. *et al.* Ide-cel or Standard Regimens in Relapsed and Refractory
483 Multiple Myeloma. *N. Engl. J. Med.* **388**, 1002–1014 (2023).
484 4. San-Miguel, J. *et al.* Cilta-cel or Standard Care in Lenalidomide-Refractory Multiple
485 Myeloma. *N. Engl. J. Med.* **389**, 335–347 (2023).
486 5. Rossi, J. *et al.* Preinfusion polyfunctional anti-CD19 chimeric antigen receptor T cells are
487 associated with clinical outcomes in NHL. *Blood* **132**, 804–814 (2018).
488 6. Fraietta, J. A. *et al.* Determinants of response and resistance to CD19 chimeric antigen
489 receptor (CAR) T cell therapy of chronic lymphocytic leukemia. *Nat. Med.* **24**, 563–571
490 (2018).
491 7. Deng, Q. *et al.* Characteristics of anti-CD19 CAR T cell infusion products associated with
492 efficacy and toxicity in patients with large B cell lymphomas. *Nat. Med.* **26**, 1878–1887
493 (2020).
494 8. Finney, O. C. *et al.* CD19 CAR T cell product and disease attributes predict leukemia
495 remission durability. *J. Clin. Invest.* **129**, 2123–2132 (2019).
496 9. Good, Z. *et al.* Post-infusion CAR TReg cells identify patients resistant to CD19-CAR
497 therapy. *Nat. Med.* **28**, 1860–1871 (2022).
498 10. Schuster, S. J. *et al.* Tisagenlecleucel in adult relapsed or refractory diffuse large B-cell
499 lymphoma. *N. Engl. J. Med.* **380**, 45–56 (2019).
500 11. Cheng, J. *et al.* Understanding the Mechanisms of Resistance to CAR T-Cell Therapy in
501 Malignancies. *Frontiers in Oncology* vol. 9 1237 (2019).

502 12. Haradhvala, N. J. *et al.* Distinct cellular dynamics associated with response to CAR-T
503 therapy for refractory B cell lymphoma. *Nat. Med.* **28**, 1848–1859 (2022).
504 13. Crouse, J., Kalinke, U. & Oxenius, A. Regulation of antiviral T cell responses by type I
505 interferons. *Nature Reviews Immunology* vol. 15 231–242 (2015).
506 14. Musella, M., Manic, G., De Maria, R., Vitale, I. & Sistigu, A. Type-I-interferons in infection
507 and cancer: Unanticipated dynamics with therapeutic implications. *Oncoimmunology* **6**,
508 1–12 (2017).
509 15. Ning, S., Pagano, J. S. & Barber, G. N. IRF7: Activation, regulation, modification and
510 function. *Genes and Immunity* vol. 12 399–414 (2011).
511 16. Curtsinger, J. M., Valenzuela, J. O., Agarwal, P., Lins, D. & Mescher, M. F. Cutting Edge:
512 Type I IFNs Provide a Third Signal to CD8 T Cells to Stimulate Clonal Expansion and
513 Differentiation. *J. Immunol.* **174**, 4465–4469 (2005).
514 17. Ramos, H. J. *et al.* Reciprocal responsiveness to interleukin-12 and interferon-α specifies
515 human CD8+ effector versus central memory T-cell fates. *Blood* **113**, 5516–5525 (2009).
516 18. Lukhele, S. *et al.* The transcription factor IRF2 drives interferon-mediated CD8+ T cell
517 exhaustion to restrict anti-tumor immunity. *Immunity* **55**, 2369-2385.e10 (2022).
518 19. Sumida, T. S. *et al.* Type I interferon transcriptional network regulates expression of
519 coinhibitory receptors in human T cells. *Nat. Immunol.* **23**, 632–642 (2022).
520 20. Harrer, D. C. *et al.* CAR Triggered Release of Type-1 Interferon Limits CAR T-Cell
521 Activities by an Artificial Negative Autocrine Loop. *Cells* **11**, (2022).
522 21. Evgin, L. *et al.* Oncolytic virus-derived type I interferon restricts CAR T cell therapy. *Nat.*
523 *Commun.* **11**, 1–15 (2020).
524 22. Musella, M., Manic, G., De Maria, R., Vitale, I. & Sistigu, A. Type-I-interferons in infection
525 and cancer: Unanticipated dynamics with therapeutic implications. *Oncoimmunology* **6**,
526 1–12 (2017).
527 23. Jakimovski, D., Kolb, C., Ramanathan, M., Zivadinov, R. & Weinstock-Guttman, B.

528 Interferon β for Multiple Sclerosis. *Cold Spring Harb. Perspect. Med.* **8**, 1–19 (2018).
529 24. Li, S. F. *et al.* Type i interferons: Distinct biological activities and current applications for
530 viral infection. *Cellular Physiology and Biochemistry* vol. 51 2377–2396 (2018).
531 25. Cho, S. S. *et al.* Activation of STAT4 by IL-12 and IFN-alpha: evidence for the
532 involvement of ligand-induced tyrosine and serine phosphorylation. *J. Immunol.* **157**,
533 (1996).
534 26. Huber, J. P., Ramos, H. J., Gill, M. A. & Farrar, J. D. Cutting Edge: Type I IFN Reverses
535 Human Th2 Commitment and Stability by Suppressing GATA3. *J. Immunol.* **185**, 813–
536 817 (2010).
537 27. Ramgolam, V. S., Sha, Y., Jin, J., Zhang, X. & Markovic-Plese, S. IFN-β Inhibits Human
538 Th17 Cell Differentiation. *J. Immunol.* **183**, 5418–5427 (2009).
539 28. Mendoza, J. L. *et al.* The IFN-λ-IFN-λR1-IL-10Rβ Complex Reveals Structural Features
540 Underlying Type III IFN Functional Plasticity. *Immunity* **46**, 379–392 (2017).
541 29. Marie, I., Durbin, J. & Levy, D. Differential viral induction of distinct interferon-alpha genes
542 by positive feedback through interferon regulatory factor-7. *EMBO J.* **17**, 6660–6669
543 (1998).
544 30. Durgin, J., Sannecy, A., Kelly, A., O'Connor, R. S. & Ghassemi, S. Type I Interferon
545 Blockade Enhances Transduction Efficiency and Efficacy of Non-Activated CAR T Cells.
546 *Blood* **142**, 6830–6830 (2023).
547 31. Cheon, H. J., Wang, Y., Wightman, S. M., Jackson, M. W. & Stark, G. R. How cancer
548 cells make and respond to interferon-I. *Trends in Cancer* **9**, 83–92 (2023).
549 32. Alizadeh, D. *et al.* IL15 enhances CAR-T cell antitumor activity by reducing mTORC1
550 activity and preserving their stem cell memory phenotype. *Cancer Immunol. Res.* **7**, 759–
551 772 (2019).
552 33. Li, L. *et al.* Transgenic expression of IL-7 regulates CAR-T cell metabolism and enhances
553 in vivo persistence against tumor cells. *Sci. Rep.* **12**, 1–14 (2022).

554 34. Štach, M. *et al.* Inducible secretion of IL-21 augments anti-tumor activity of piggyBac-
555 manufactured chimeric antigen receptor T cells. *Cytotherapy* **22**, 744–754 (2020).
556 35. Zhao, Y. *et al.* IL-10-expressing CAR T cells resist dysfunction and mediate durable
557 clearance of solid tumors and metastases. *Nat. Biotechnol.* (2024) doi:10.1038/s41587-
558 023-02060-8.
559 36. Feng, B. *et al.* The type 2 cytokine Fc–IL-4 revitalizes exhausted CD8+ T cells against
560 cancer. *Nature* **634**, (2024).
561 37. Berraondo, P. *et al.* Cytokines in clinical cancer immunotherapy. *Br. J. Cancer* **120**, 6–15
562 (2019).
563 38. Buchwalder, P., Buclin, T., Trinchard, I., Munafo, A. & Biollaz, J. Pharmacokinetics and
564 Pharmacodynamics of IFN-b1a in Healthy Volunteers. *J. Interf. Cytokine Res.* **20**, 857–
565 866 (2000).
566 39. Davis, A. M., Ramos, H. J., Davis, L. S. & Farrar, J. D. Cutting Edge: A T-bet-
567 Independent Role for IFN-α/β in Regulating IL-2 Secretion in Human CD4 + Central
568 Memory T Cells. *J. Immunol.* **181**, 8204–8208 (2008).
569 40. van Boxel-Dezaire, A. H. H., Rani, M. R. S. & Stark, G. R. Complex Modulation of Cell
570 Type-Specific Signaling in Response to Type I Interferons. *Immunity* **25**, 361–372 (2006).
571 41. Jung, I. Y. *et al.* Type I Interferon Signaling via the EGR2 Transcriptional Regulator
572 Potentiates CAR T Cell–Intrinsic Dysfunction. *Cancer Discov.* **13**, 1636–1655 (2023).
573 42. Ng, C. T., Mendoza, J. L., Garcia, K. C. & Oldstone, M. B. A. Alpha and Beta Type 1
574 Interferon Signaling: Passage for Diverse Biologic Outcomes. *Cell* **164**, 349–352 (2016).
575 43. Zhao, Z. *et al.* Structural Design of Engineered Costimulation Determines Tumor
576 Rejection Kinetics and Persistence of CAR T Cells. *Cancer Cell* **28**, 415–428 (2015).
577 44. Elewaut, A. *et al. Cancer cells impair monocyte-mediated T cell stimulation to evade*
578 *immunity. Nature* vol. 637 (Springer US, 2024).
579 45. Sun, Y. *et al.* The downregulation of type I IFN signaling in G-MDSCs under tumor

580 conditions promotes their development towards an immunosuppressive phenotype. *Cell*
581 *Death Dis.* **13**, 1–13 (2022).
582 46. Alicea-Torres, K. *et al.* Immune suppressive activity of myeloid-derived suppressor cells
583 in cancer requires inactivation of the type I interferon pathway. *Nat. Commun.* **12**, (2021).
584 47. Hao, Y. *et al.* Integrated analysis of multimodal single-cell data. *Cell* **184**, 3573-3587.e29
585 (2021).
586 48. Korsunsky, I. *et al.* Fast, sensitive and accurate integration of single-cell data with
587 Harmony. *Nat. Methods* **16**, 1289–1296 (2019).
588 49. Wu, T. *et al.* clusterProfiler 4.0: A universal enrichment tool for interpreting omics data.
589 *Innovation* **2**, (2021).
590 50. Subramanian, A. *et al.* Gene set enrichment analysis: A knowledge-based approach for
591 interpreting genome-wide expression profiles. *Proc. Natl. Acad. Sci. U. S. A.* **102**, 15545–
592 15550 (2005).
593 51. Cao, G. *et al.* Two-stage CD8+ CAR T-cell differentiation in patients with large B-cell
594 lymphoma. *Nat. Commun.* **16**, 4205 (2025).
595

MAIN FIGURES AND LEGENDS

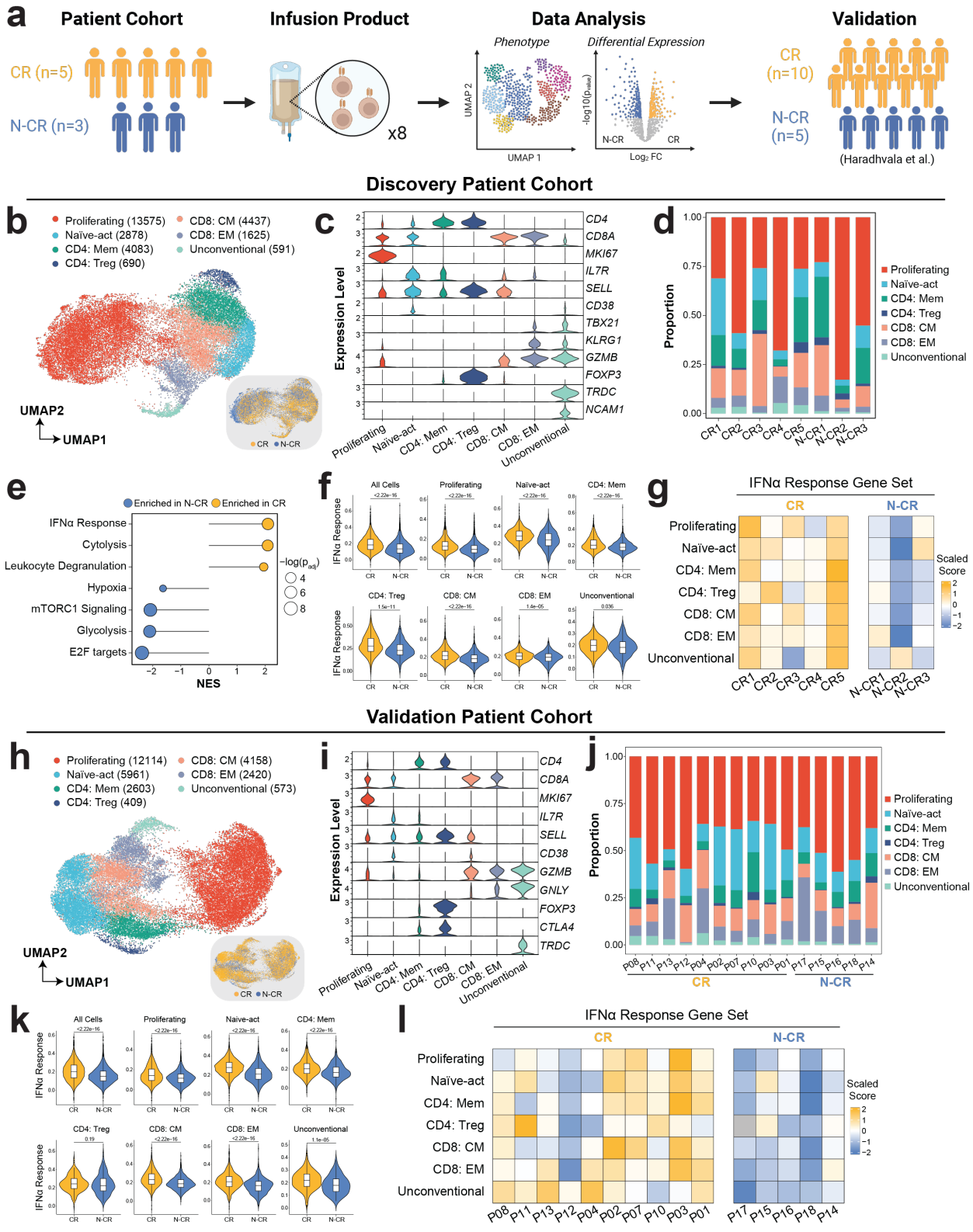

Figure 1. Enrichment of IFN-I signaling in infusion products of complete responders. (**a**) Cartoon depicting study design of single-cell analysis on infusion products of patients who received axi-cel from discovery dataset and validation datasets. CR, complete responder, N-CR, non-complete responder. (**b**) UMAP demonstrating 7 T-cell clusters in infusion product from discovery dataset. (**c**) Violin plots depicting normalized expression levels of representative markers for each cluster. (**d**) Stacked bar graphs depicting T-cell cluster proportions for each patient in discovery dataset. (**e**) Gene set enrichment analysis comparing CR and N-CR T cells. For each gene set, direction and statistical significance of enrichment are indicated by the circle's color and size, respectively. (**f**) Violin plots depicting IFNα response signature scores in CR and N-CR T cells from each T-cell cluster. Signature scores were compared by Wilcoxon Rank-Sum test. (**g**) Tilemap depicting scaled IFNα response signature scores in each T-cell cluster across patients. (**h**) UMAP demonstrating 7 T-cell clusters in infusion product from validation dataset from Maus et al. (**i**) Violin plots depicting normalized expression levels of representative markers for each cluster. (**j**) Stacked bar graphs depicting T-cell cluster proportions for each patient in validation dataset. (**k**) Violin plots depicting signature scores in CR and N-CR T cells from each T-cell cluster. Signature scores were compared by Wilcoxon Rank-Sum test. (**l**) Tilemap depicting scaled signature scores of IFNα response gene sets in each T-cell cluster across patients. No Treg was found in P17 infusion products, colored in gray.

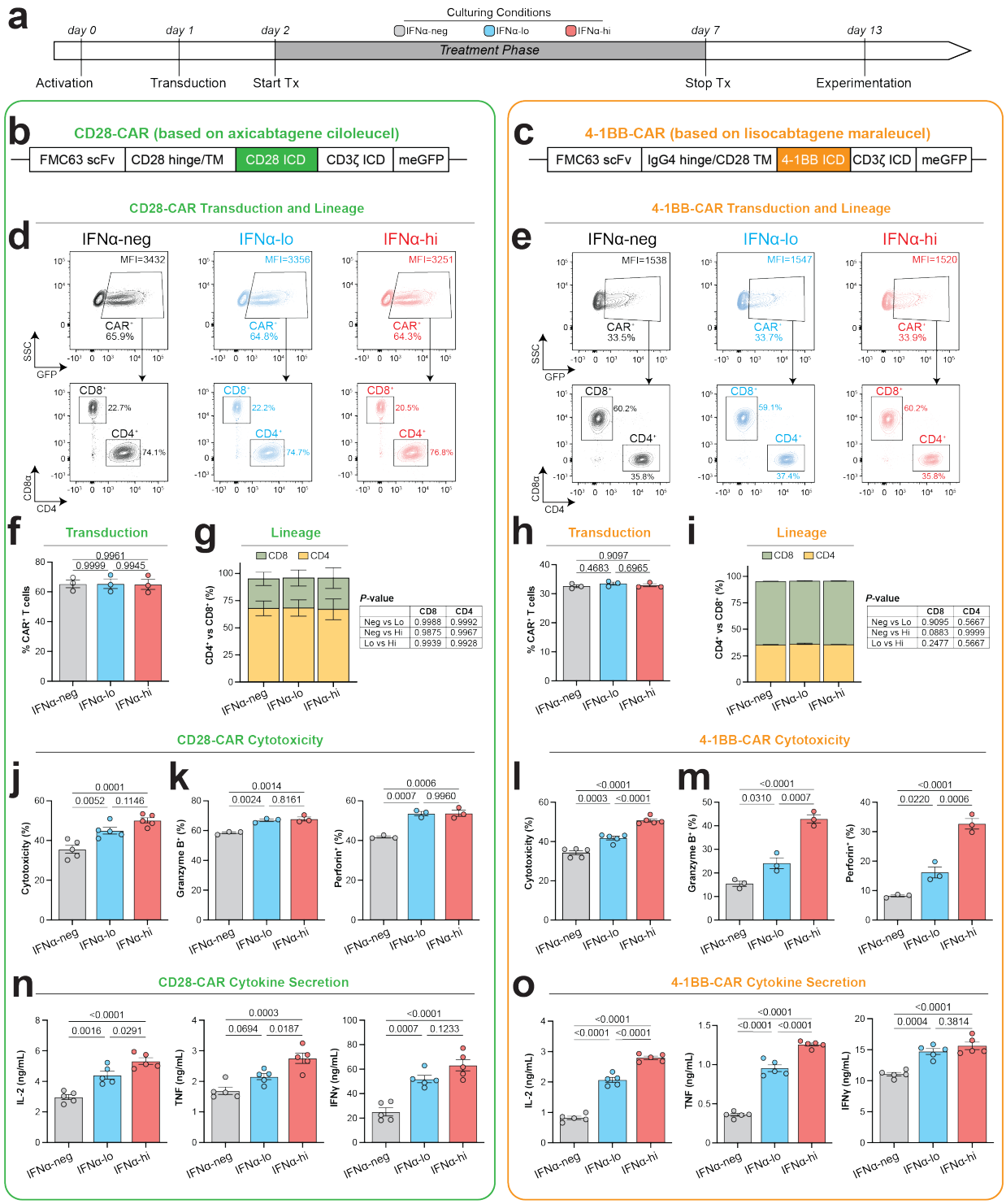
a
Culturing Conditions
IFNα-neg
IFNα-lo
IFNα-hi
day 0
day 1
day 2
day 7
day 13
Treatment Phase
Activation
Transduction
Start Tx
Stop Tx
Experimentation
b
CD28-CAR (based on axicabtagene ciloleucel)
FMC63 scFv
CD28 hinge/TM
CD28 ICD
CD3ζ ICD
meGFP
c
4-1BB-CAR (based on lisocabtagene maraleucel)
FMC63 scFv
IgG4 hinge/CD28 TM
4-1BB ICD
CD3ζ ICD
meGFP
CD28-CAR Transduction and Lineage
4-1BB-CAR Transduction and Lineage
d
e
IFNα-neg
IFNα-lo
IFNα-hi
MFI=3432
MFI=3356
MFI=3251
MFI=1538
MFI=1547
MFI=1520
CAR+ 65.9%
CAR+ 64.8%
CAR+ 64.3%
CAR+ 33.5%
CAR+ 33.7%
CAR+ 33.9%
SSC
GFP
CD8+ 22.7%
CD4+ 74.1%
CD8+ 22.2%
CD4+ 74.7%
CD8+ 20.5%
CD4+ 76.8%
CD8+ 60.2%
CD4+ 35.8%
CD8+ 59.1%
CD4+ 37.4%
CD8+ 60.2%
CD4+ 35.8%
CD8α
CD4
f
Transduction
% CAR+ T cells
0.9961
0.9999
0.9945
IFNα-neg
IFNα-lo
IFNα-hi
g
Lineage
CD8
CD4
CD4+ vs CD8+ (%)
P-value
CD8 CD4
Neg vs Lo 0.9988 0.9992
Neg vs Hi 0.9875 0.9967
Lo vs Hi 0.9939 0.9928
h
Transduction
% CAR+ T cells
0.9097
0.4683
0.6965
i
Lineage
CD4+ vs CD8+ (%)
P-value
CD8 CD4
Neg vs Lo 0.9095 0.5667
Neg vs Hi 0.0883 0.9999
Lo vs Hi 0.2477 0.5667
CD28-CAR Cytotoxicity
4-1BB-CAR Cytotoxicity
j
Cytotoxicity (%)
0.0001
0.0052
0.1146
k
Granzyme B+ (%)
0.0014
0.0024
0.8161
Perforin+ (%)
0.0006
0.0007
0.9960
l
Cytotoxicity (%)
<0.0001
0.0003
<0.0001
m
Granzyme B+ (%)
<0.0001
0.0310
0.0007
Perforin+ (%)
<0.0001
0.0220
0.0006
n
CD28-CAR Cytokine Secretion
IL-2 (ng/mL)
<0.0001
0.0016
0.0291
TNF (ng/mL)
0.0003
0.0694
0.0187
IFNγ (ng/mL)
<0.0001
0.0007
0.1233
o
4-1BB-CAR Cytokine Secretion
IL-2 (ng/mL)
<0.0001
<0.0001
<0.0001
TNF (ng/mL)
<0.0001
<0.0001
<0.0001
IFNγ (ng/mL)
<0.0001
0.0004
0.3814

616

617 **Figure 2. IFN-I signaling increases CAR T-cell cytotoxicity.**
618 (**a**) Workflow of CAR T-cell ex vivo generation, treatment, and culturing. (**b**-**c**) CD28- or 4-1BB-
619 costimulated CAR designs based on the construct used in axicabtagene ciloleucel (**b**) or
620 lisocabtagene maraleucel, respectively (**c**). (**d**-**e**) Representative flow plots depicting gating for
621 CAR expression (top) and T-cell lineages (bottom) in CD28-costimulated (**d**) and 4-1BB-
622 costimulated (**e**) CAR T cells. (**f**, **h**) Transduction percentage as measured by meGFP
623 fluorescence among T cells from each culturing condition in CD28-costimulated (**f**, n=3) and 4-
624 1BB-costimulated (**h**, n=3) CAR T cells. (**g**, **i**) Stacked bar plot comparing CD8 vs CD4 proportions
625 in CD28-costimulated (**g**, n=3) and 4-1BB-costimulated (**i**, n=3) CAR T cells. (**j**-**m**) Cytotoxicity of
626 CD28-costimulated (**j**-**k**) and 4-1BB-costimulated (**l**-**m**) CAR T cells. (**j**, **l**) direct cytotoxicity against
627 firefly luciferase-expressing OCI-Ly8 target cells at E/T ratio of 1:1 via 6-hr bioluminescence assay
628 (n=5). (**k**, **m**) intracellular staining for granzyme B (right) and perforin (left) after 4-hr of coculture
629 with OCI-Ly8 at E/T ratio of 1:1 as measured by flow cytometry (n=3). (**n**-**o**) Concentration of
630 cytokines secreted by CD28-costimulated (**n**) and 4-1BB-costimulated (**o**) CAR T cells into the
631 supernatant after 24-hr of coculture with OCI-Ly8 at E/T ratio of 1:1 as measured by ELISA (n=5).
632 From left to right, IL-2, TNF, and IFNγ. All data are reported as mean ± standard error. Statistical
633 analysis were performed via one-way (**f**, **h**, **j**-**o**) or two-way (**g**, **i**) ANOVA with Tukey correction for
634 multiple comparisons. All panels are representative data from 3 independent donors.

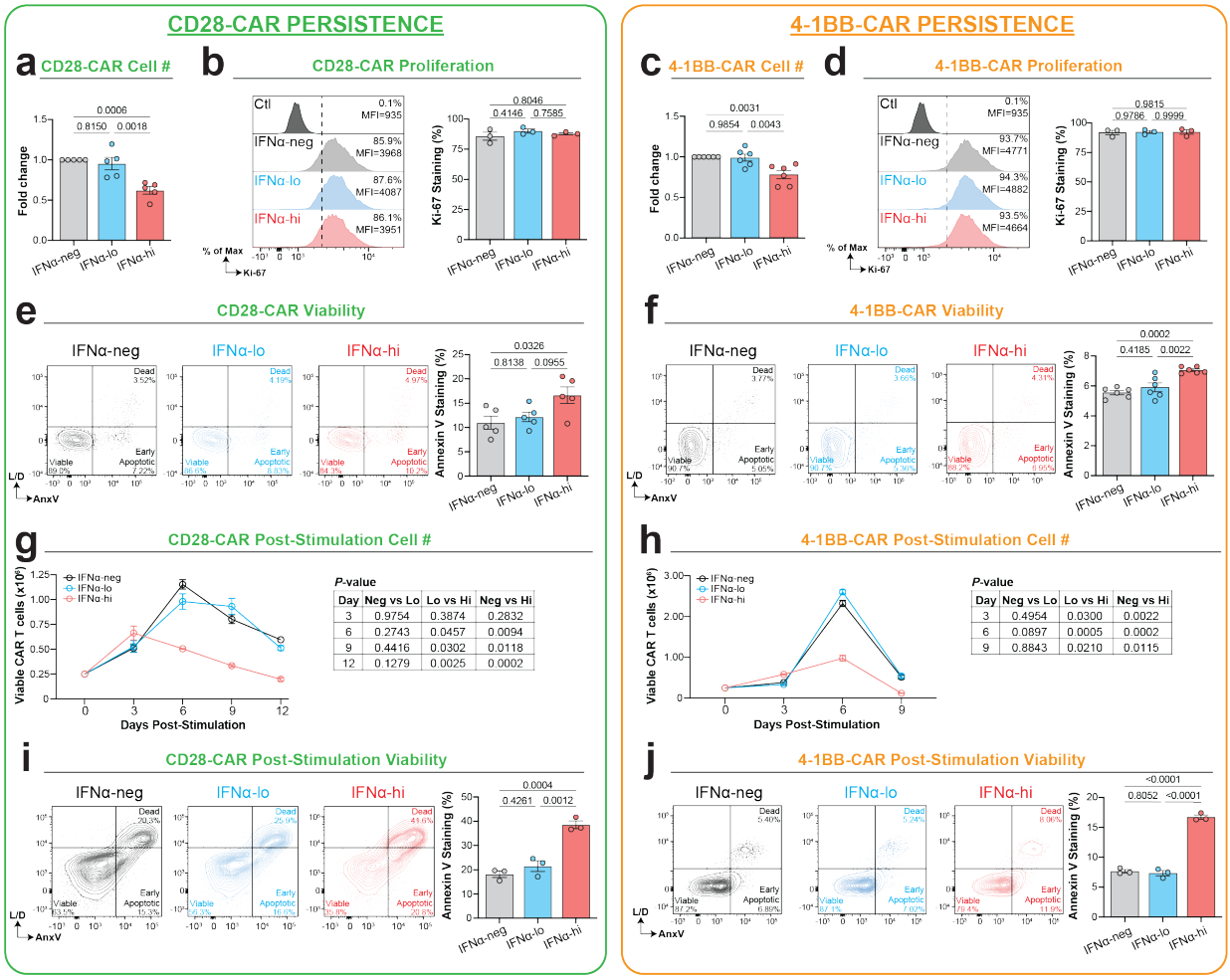
CD28-CAR PERSISTENCE
a CD28-CAR Cell #
b CD28-CAR Proliferation
e CD28-CAR Viability
g CD28-CAR Post-Stimulation Cell #
i CD28-CAR Post-Stimulation Viability
4-1BB-CAR PERSISTENCE
c 4-1BB-CAR Cell #
d 4-1BB-CAR Proliferation
f 4-1BB-CAR Viability
h 4-1BB-CAR Post-Stimulation Cell #
j 4-1BB-CAR Post-Stimulation Viability
IFNα-neg
IFNα-lo
IFNα-hi
Fold change
Ki-67 Staining (%)
Annexin V Staining (%)
Viable CAR T cells (x10⁶)
Days Post-Stimulation
P-value
Day | Neg vs Lo | Lo vs Hi | Neg vs Hi
3 | 0.9754 | 0.3874 | 0.2832
6 | 0.2743 | 0.0457 | 0.0094
9 | 0.4416 | 0.0302 | 0.0118
12 | 0.1279 | 0.0025 | 0.0002
P-value
Day | Neg vs Lo | Lo vs Hi | Neg vs Hi
3 | 0.4954 | 0.0300 | 0.0022
6 | 0.0897 | 0.0005 | 0.0002
9 | 0.8843 | 0.0210 | 0.0115

635

636 **Figure 3. High-strength IFN-I signaling increases apoptosis, whereas low-strength IFN-I**
637 **signaling does not.**
638 (**a**, **c**) Relative counts of live CAR T cells from the three culturing conditions after CAR T-cell
639 manufacturing in CD28-costimulated (**a**, n=5) and 4-1BB-costimulated (**c**, n=6) CAR T cells.
640 Counts were normalized to the IFNα-neg condition. (**b**, **d**) Proliferation of CAR T cells from the
641 three culturing conditions in CD28-costimulated (**b**, n=3) and 4-1BB-costimulated (**d**, n=3) CAR T
642 cells. Left, representative flowplots depicting gating for Ki-67^{+} proliferating CAR T cells at the day
643 when IFNα was removed. Right, Ki-67^{+} proliferating cell proportions among CAR T cells. Non-
644 activated naïve T cells from human PBMCs were used as a biological control for gating. (**e**, **f**)
645 Apoptosis of CAR T cells from the three culturing conditions after CAR T-cell manufacturing in
646 CD28-costimulated (**a**, n=5) and 4-1BB-costimulated (**c**, n=6) CAR T cells. Left, representative
647 flow plots depicting gating for viable, early apoptotic, and dead cells among CAR T cells. Right,
648 staining for Annexin V positivity among live CAR T cells. (**g**, **h**) Line graphs depicting viable CAR
649 T-cell cellularity of CD28-costimulated (**g**, n=3) and 4-1BB-costimulated (**h**, n=3) CAR T cells in
650 vitro following coculture with OCI-Ly8 at E/T ratio of 1:5. (**i**, **j**) Apoptosis of CD28-costimulated
651 CAR T cells (**i**, n=3) and 4-1BB-costimulated CAR T cells (**j**, n=3) from the three culturing
652 conditions at day 6 after coculture with OCI-Ly8 cells at E/T ratio of 1:5. Left, representative flow
653 plots depicting gating for viable, early apoptotic, and dead cells among the three culturing
654 conditions. Right, staining for Annexin V positivity among live CAR T cells. All data are reported
655 as mean ± standard error. Statistical analysis were performed via one-way (**a**-**f**, **i**-**j**) or two-way (**g**,
656 **h**) ANOVA with Tukey correction for multiple comparisons. Panels **a**, **c**, **e**-**j** are representative data
657 from 3 independent donors. Panels **b**, **d** are representative data from 2 independent donors.

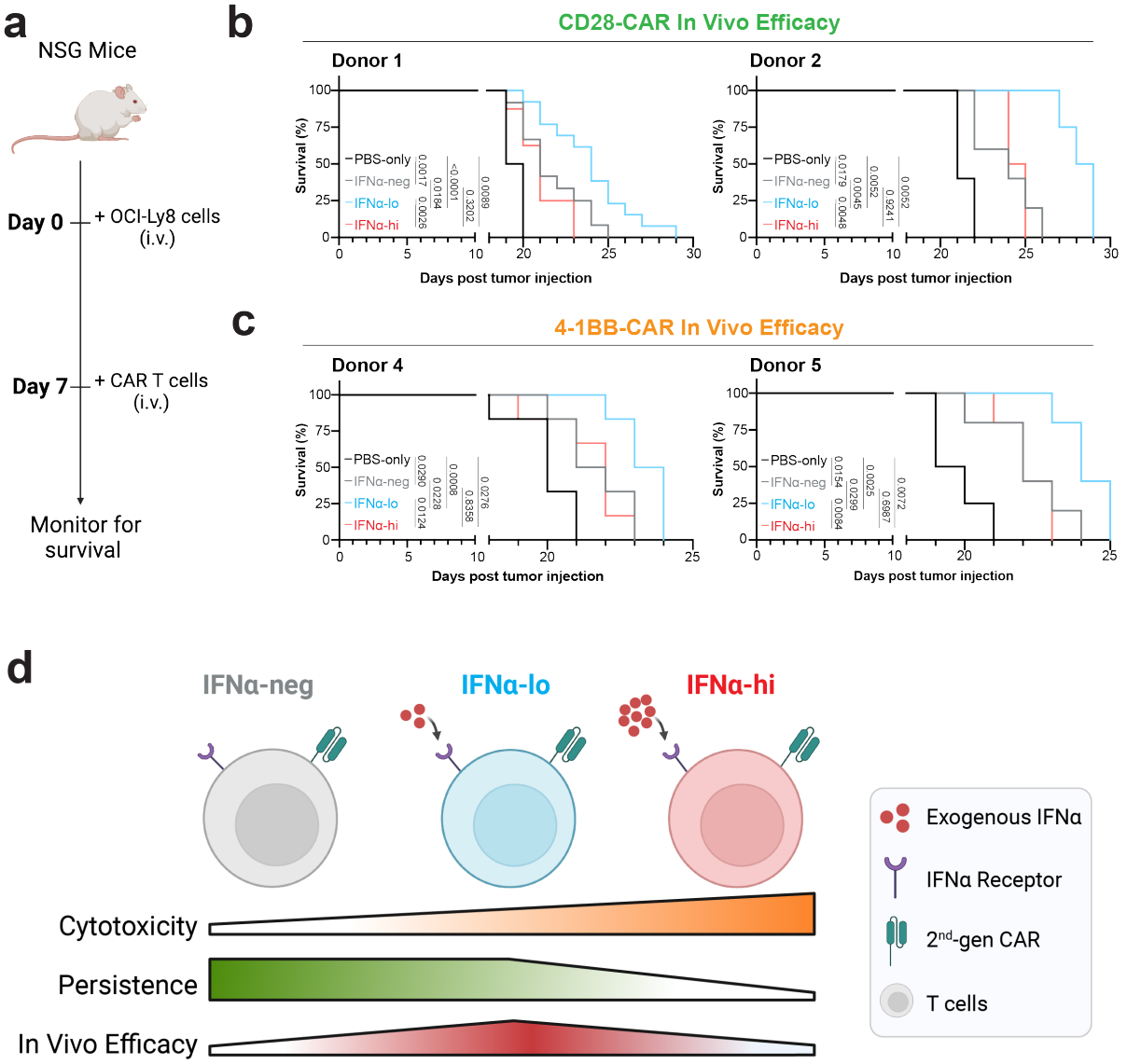

Figure 4. Low-strength IFN-I signaling promotes CAR T-cell treatment efficacy in vivo. (**a**) Schematic depicting timeline for NSG mouse model based on OCI-Ly8 lymphoma cell line. Seven days following OCI-Ly8 injection, mice were randomly divided into groups that were treated with either PBS or CAR T cells from the three culturing conditions. (**b**) Kaplan-Meier analysis of survival of OCI-Ly8-bearing mice treated with PBS or 5×10^5 CD28-costimulated CAR T cells from various culture conditions. CAR T cells were generated from donor 1 (left, n=8,12,13,8), and donor 2 (right, n=5,5,4,4). (**c**) Kaplan-Meier analysis of survival of OCI-Ly8-bearing mice treated with PBS or 5×10^5 (left) or 1×10^6 (right) 4-1BB-costimulated CAR T cells from various culture conditions. CAR T cells were generated from donor 4 (left, n=6,6,6,6), and donor 5 (right, n=4,5,5,5). (**d**) Cartoon summarizing effects of IFN-I signaling on CAR T cells at different doses. Statistical analysis were performed by log-rank (Mantel-Cox) test.